Structure of the Zinc Transporter YiiP

Min Lu and Dax Fu*

YiiP is a membrane transporter that catalyzes Zn^{2+}/H^{+} exchange across the inner membrane of *Escherichia coli*. Mammalian homologs of YiiP play critical roles in zinc homeostasis and cell signaling. Here, we report the x-ray structure of YiiP in complex with zinc at 3.8 angstrom resolution. YiiP is a homodimer held together in a parallel orientation through four Zn^{2+} ions at the interface of the cytoplasmic domains, whereas the two transmembrane domains swing out to yield a Y-shaped structure. In each protomer, the cytoplasmic domain adopts a metallochaperone-like protein fold; the transmembrane domain features a bundle of six transmembrane helices and a tetrahedral Zn^{2+} binding site located in a cavity that is open to both the membrane outer leaflet and the periplasm.

Zinc is essential for cellular growth and differentiation. The total zinc content in a living cell is sustained at submillimolar levels, mostly in a protein-bound form (*1*). The ligated zinc can serve as catalytic or structural cofactors in a host of biological processes ranging from gene expression to immune functions (*2*). A pool of loosely bound zinc in the brain plays an additional role in modulating neurotransmission (*3*). Presynaptic vesicles of glutamatergic neurons and insulin-containing secretory vesicles of pancreatic β cells are particularly rich in zinc, with concentrations exceeding 1 mM (*4*, *5*). Although zinc is abundant in certain specialized subcellular organelles, abnormally elevated zinc concentrations in the cytoplasm may exert cytotoxic effects. For instance, excessive zinc may contribute to neuronal cell death during brain ischemia (*6*) and to β-amyloid deposition in Alzheimer's disease (*7*, *8*). Therefore, the free cytoplasmic zinc concentration of a living cell is maintained well below the nanomolar level (*9*).

A family of ubiquitous zinc transporters, termed cation diffusion facilitator (CDF), is critically involved in controls of cytoplasmic zinc build-ups, either by facilitating zinc efflux to the cell exterior or by accumulating the excess zinc in intracellular storage organelles (*10*, *11*). These zinc transporters move Zn^{2+} across the otherwise impermeable membrane barriers. In glutamatergic synapses, a mammalian CDF, known as ZnT-3 (zinc transporter-3), is responsible for sequestering cytoplasmic Zn^{2+} into presynaptic vesicles (*12*). In pancreatic β cells, yet another mammalian CDF, ZnT-8 (*SLC30A8*), stimulates zinc accumulation in the insulin secretory vesicles (*13*). Emerging evidence has linked ZnT-8 to the pathogenesis of type 2 diabetes (*14*). At present, little is known about the structure and molecular mechanism of ZnTs. Three bacterial CDF homologs, YiiP and ZitB from *Escherichia coli* and CzcD from *Ralstonia metallidurans*, have been characterized functionally and are related to their mammalian counterparts with 25 to 30% sequence identity (Fig. 1). YiiP is a homodimer of two 33-kD integral membrane proteins (*15*), each composed of six transmembrane segments (TMs) and a hydrophilic C-terminal domain (CTD) located in the cytoplasm (*16*). Metal binding and transport by YiiP have been mapped to strictly conserved D49 and D157 in the transmembrane domain (TMD) with binding affinities for Zn^{2+} and Cd^{2+} in the submicromolar range (*17*). The transcription of *yiiP* gene in *E. coli* is inducible by both Zn^{2+} and Fe^{2+} (*18*, *19*), although YiiP expression seems to promote iron detoxification only. However, direct transport measurement using native membrane vesicles indicated that YiiP catalyzes Zn^{2+}/H^{+} antiport (*19*).

We obtained YiiP crystals following an extensive screening for crystallization conditions. Although several metal ions improved the stability of YiiP in detergent micelles, only Zn^{2+} yielded crystals of diffraction quality. X-ray diffraction data were obtained from native crystals and 12 heavy-atom derivative crystals for multiple isomorphous replacement and anomalous scattering phasing (table S1) (*20*). The resulting experimental maps to 3.8 Å revealed two YiiP protomers per asymmetric unit, one of which could be readily traced as a continuous polypeptide chain (figs. S1 and S2), whereas the other is more disordered as a result of less favorable crystal contacts. Protein sequence registration was established by using electron densities for bulky side chains and 11 major heavy metal binding sites (table S2). Subsequent structure refinement and model rebuilding resulted in a structural model with R_{cryst} and R_{free} of 32.2% and 32.9%, respectively. The final model contained all but the first 4 and the last 10 residues of the 300 amino acids in each protomer.

The physiological YiiP homodimer is arranged around a two-fold crystallographic axis oriented perpendicular to the membrane plane (Fig. 2A). Two bands of aromatic residues on the protein surface suggest the boundaries of the membrane-embedded region. The CTDs protrude into the cytoplasm and juxtapose each other in parallel to form the major dimerization contact. At the CTD and TMD juncture, intracellular loops form another dimerization contact, from which two TMDs swing outward and plunge into the membrane with a 60° crossing angle. Viewed from the membrane plane, this dimeric structure exhibits a Y-shaped architecture, with each arm formed by a TMD; the bulk of the Y stem is provided by the associated CTDs. Given this orientation within

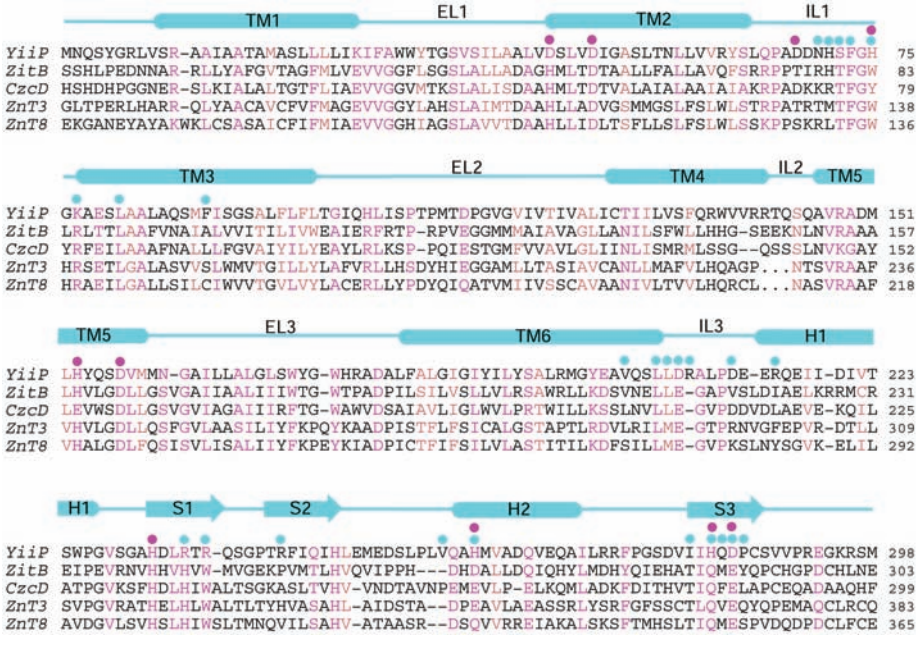

Fig. 1. Sequence alignment of YiiP and representative members of the CDF protein family. Conserved and homologous residues are colored in magenta and light-brown respectively. Regions of secondary structural elements in YiiP are outlined. Magenta and cyan dots indicate residues involved in Zn^{2+} binding and dimerization contacts, respectively. Dots within the two human sequences indicate omitted residues in a loop (IL2) between TM4 and TM5. The signature sequence suggested for the CDF family corresponds to the aligned YiiP sequence from residues 36 to 49 (*27*).

Department of Biology, Brookhaven National Laboratory, Upton, NY 11973, USA.

*To whom correspondence should be addressed. E-mail: dax@bnl.gov

the membrane, the void space observed between two TMDs is likely to be filled with phospholipids in vivo. Viewed from extracellular side down the two-fold axis (Fig. 2B), the lower protein density between TMDs is consistent with a distinctive constriction of electron density at the dimer interface of a YiiP projection map obtained in the native *E. coli* lipid bilayer (*15*).

Residues from 1 to 211 of YiiP are folded into the TMD as a compact six-helix bundle (Fig. 2). Interdigitations of helices in YiiP all fall into the "knobs-into-holes" type of contact, and the crossing angles between helices are within the optimal range. A lack of helix-breaking proline residues in the middle of transmembrane helices suggests a rather limited conformational flexibility in the TMD. Threading across the membrane six times, transmembrane helices are linked together by three extracellular loops, denoted as EL1 to EL3, and two intracellular loops, IL1 and IL2 (Fig. 1). An additional intracellular loop, IL3, connects TM6 to the CTD. IL1 extends toward the dimer interface and forms a dimerization contact with IL3 from the neighboring subunit (Fig. 2B). Related by the two-fold symmetry, IL3 and IL1 of the neighboring subunit form another dimerization contact. IL2 makes a short connection between TM4 and TM5, with only four residues from position 141 to 144 (Fig. 2A).

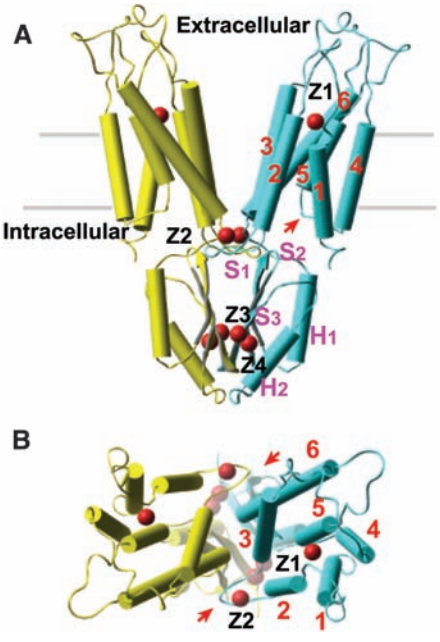

Fig. 2. YiiP with bound Zn^{2+}. (**A**) YiiP homodimer (yellow and cyan for each protomer) viewed from the membrane plane. Zn^{2+} ions are represented by red spheres and labeled as Z1 to Z4. Transmembrane helixes are numbered 1 to 6, α helices and β strands in CTD are labeled as H1 and H2, and S1 to S3, respectively. IL2 is indicated by an arrow. (**B**) View from the extracellular side along the membrane normal. Dimerization contacts between IL1 and IL3 are indicated by arrows.

The length of TM5 is conspicuously short, accounting for three and a half helical turns from residue V147 to M159. This short helix is largely sequestered in the center of the six-helix bundle, thereby giving rise to one extracellular and one intracellular cavity on either side of the membrane (Fig. 3A). The extracellular cavity is accessible from the bulk solvent and exposed to the membrane outer leaflet (Fig. 3C). This cavity spans nearly half of the membrane thickness and anchors a Zn^{2+} ion near the bottom. The intracellular cavity is confined between the TMD and CTD (Fig. 3A). The extended IL1 and IL3 partially obstruct lateral solvent accessibility to the cavity along the cytoplasmic face of the membrane, while the short IL2 makes room for full solvent access from the distal side of the dimer interface. The dome of the intracellular cavity is capped by three highly conserved residues at the amino end of TM5, V147, R148, and A149. Directly under the dome lie the conserved R11 from TM1, E79 from TM3, E200 from TM6, and a variable Q145 from IL2 (Fig. 3D). The two cavities are open to different sides of the membrane and point toward each other within the membrane, but no connecting channel exists between them (Fig. 3B).

Residues from 212 to 300 of CTD are folded into an open α-β domain with two α helices (H1 and H2) aligned on one side and a three-stranded mixed β sheet (S1 to S3) on the other side (fig. S3). The CTD exhibits an overall structural similarity with the copper metallochaperone Hah1 (*21*), although there is no sequence homology between CTD and Hah1. To a first approximation, the topologies of the CTD αβ-βαβ and the Hah1 βαβ-βαβ fold are identical except that the first β strand in Hah1 loops out as IL3 in YiiP. The αβ-βα structural core of CTD from H1 to H2 can be superimposed onto the equivalent portion of Hah1 with a root mean square deviation of 1.8 Å for 42 common Cα positions. To date, all known structures of metallochaperones and their target domains have shared a common metallochaperone-like fold (*22*, *23*). The fold of CTD places it into the same structural category as a possible Zn^{2+} receiving domain.

Anomalous difference Fourier maps of native crystals were computed using experimental phases and diffraction data collected at the zinc edge. Four strong anomalous peaks indicate the presence of four Zn^{2+}-populated sites (designated as Z1 to Z4) in each protomer (Fig. 4). Calorimetric titrations of EDTA pretreated YiiP yielded 2.6 Zn^{2+} stoichiometric units per YiiP protomer, corresponding to two Zn^{2+}-binding sites with an overall dissociation constant (K_d) of 0.24 μM and a low-affinity component (K_d = 145 μM) (*16*). The free Zn^{2+} concentration in the crystallization solution is buffered by citrate within the micromolar range (*24*); thus, only the two high-affinity sites (K_d = 0.24 μM) may have been mostly saturated to become visible in electron density maps. Anomalous peak heights from site Z1 to Z4 increase progressively from 4.6 and 5.8 to 9.6 and 9.6 σ, revealing a rank order of Zn^{2+} occupancy consistent with Z1 and Z2 as being EDTA chelatable, and Z3 and Z4 as EDTA resistant. The EDTA-resistant sites did not respond to calorimetric titrations, but they likely exist because prolonged EDTA chelation denatured YiiP (*25*).

The Zn^{2+} in site Z1 is tetracoordinated by highly conserved D45, D49 from TM2, and H153, D157 from TM5 (Fig. 4). All these res-

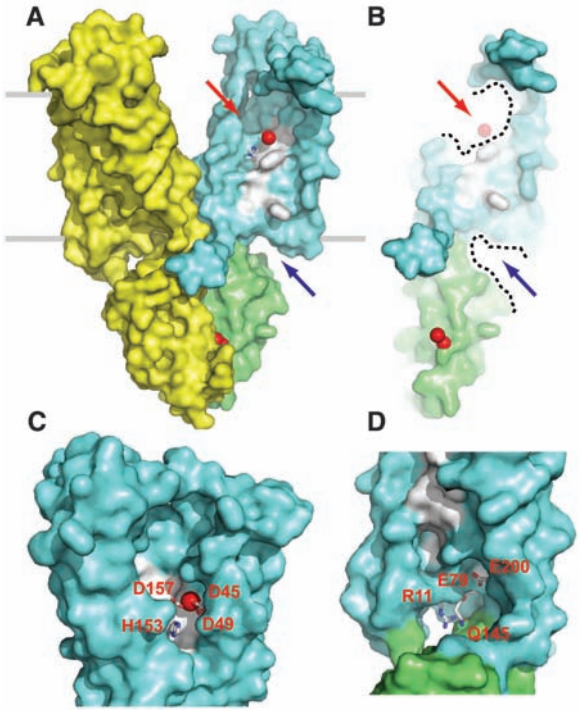

Fig. 3. Extracellular and intracellular cavities. (**A**) YiiP dimer is viewed from the membrane plane. The front portions of TM1, TM2, and CTD of one protomer (cyan) are removed to reveal the embedded TM5 (gray patch), the extracellular cavity (red arrow), and the intracellular cavity (blue arrow). TMD and CTD are colored cyan and green, respectively. (**B**) A cross section of a YiiP monomer with both the front and back portions removed to highlight the barrier that separates two cavities. The cavity boundaries are outlined by dashed lines. (**C**) Close-up view of the extracellular cavity along the red arrow. A bound Zn^{2+} near the bottom is colored red, and its coordination residues are drawn as sticks. (**D**) Close-up view of the intracellular cavity along the blue arrow, with R11, E79, Q145, and E200 drawn as sticks.

idues are essential for Zn^{2+} transport activity (*17*). The tetrahedral coordination is a preferred geometry for Zn^{2+} binding. Consistently, metal binding to cysteine substitutes of D49 and D157 is selective for Zn^{2+} and its isomorphous Cd^{2+} but discriminative against Ca^{2+}, Mg^{2+}, Ni^{2+}, Co^{2+}, and Mn^{2+}, all of which favor different coordination geometries (*16*, *17*). Site Z1 is located near the bottom of the extracellular cavity and exposed to aliphatic lipid chains, where hydrophobic mismatch between packing lipids and the irregular cavity surface may create water-filled packing defects in the lipid matrix.

The Zn^{2+} in site Z2 binds to the intracellular loop that connects TM2 and TM3 (IL1) (Fig. 4). This loop is semiconserved and harbors many potential Zn^{2+} ligating residues. Side chains in this region are not well resolved, but the primary Zn^{2+} coordination shell appears to involve D68 and H75. Additional coordination residues may complete the tetrahedral coordinate geometry. Although the functional role of site Z2 has yet to be defined, its involvement in subunit dimerization is evident. Site Z2 is adjacent to a cluster of highly conserved residues at the dimer interface, including S72 and F73 from IL1, K77 and L81 from the amino end of TM3, and L205, L206, and D207 from IL3 of the neighboring subunit. These residues make direct hydrogen bonds and Van der Waals interactions across the dimer interface.

Located within a cleft between two CTDs, sites Z3 and Z4 appear to be bridged by the highly conserved D285 through a bidentate coordination (Fig. 4). The two Zn^{2+} ions align nearly perpendicular to the long axis of the β sheet, thereby straddling all three β strands of one subunit and coordinating residues from H2 of the neighboring subunit. Unambiguous placement of side chains was not feasible in the β-sheet region, but it is evident that the binuclear Zn^{2+} binding establishes a coordination network at least involving H232 from S1, H283 and D285 from S3, and H261 from H2 of the neighboring subunit. Furthermore, a two-fold related binuclear Zn^{2+} cluster is located on the opposite side of the CTD dimer interface (Fig. 4). The positioning of two Zn^{2+} clusters and their resistance to EDTA chelation suggest a structural role that they may play in strengthening the dimerization contact.

The structure of YiiP provides a model for rationalizing mutagenic results from CzcD and ZitB (*26*) (Fig. 1). In TM1, a $CzcD^{E31k}$ mutation abolished the transport activity. The YiiP equivalent of $CzcD^{E31}$ is a membrane-embedded K27, which seems to be stabilized by D45 of site Z1. In CzcD, an H49 is in place of $YiiP^{D45}$, which is incapable of stabilizing the positive charge on $CzcD^{E31K}$. In TM2, mutations of $CzcD^{H49}$, $CzcD^{D53}$, $ZitB^{H53}$, and $ZitB^{D57}$ resulted in functionless proteins, because their YiiP equivalents (D45 and D49) contribute to site Z1. In TM4, $ZitB^{N135}$ is required for function, and its YiiP equivalent (T128) wedges between TM1 and TM5 into a hydrophobic pocket near site Z1. In TM5, mutations of $CzcD^{E154}$, $CzcD^{D158}$, $ZitB^{H159}$, and $ZitB^{D163}$ abolished transport activity, and these residues in YiiP (H153 and D157) contribute to site Z1. Near the amino end of TM6, a strictly conserved $YiiP^{D179}$ is involved in crystal contacts, obscuring its functional implications. In addition, $ZitB^{E214A}$, $CzcD^{H237R}$, and $CzcD^{H280}$ impaired transport activity. Their YiiP equivalents are all involved in dimerization contacts. The emerging pattern of structure-function correlation is the clustering of loss-of-function mutations around site Z1 and the dimer interface. Although two TMDs in the YiiP structure swing out as separated transmembrane units, dimerization seems essential for YiiP function.

The low-resolution YiiP structure is characterized by two water-filled cavities, which collectively penetrate more than half of the membrane thickness from opposite membrane surfaces. The tetrahedral Zn^{2+} binding site (site Z1) near the bottom of the extracellular cavity is separated from a cluster of conserved residues located near the dome of the intracellular cavity. Although no Zn^{2+} binding was observed within the intracellular cavity of the current structure, a similar cation (Cd^{2+}) can be placed at the cavity entrance by superimposing one subunit of an Hah1-Cd^{2+}-Hah1 dimer onto the YiiP CTD. We propose that the binding of a putative Zn^{2+} metallochaperone to YiiP CTD may deliver a cytoplasmic Zn^{2+} to the intracellular cavity where the Zn^{2+} is then translocated across the membrane to site Z1 in the extracellular cavity.

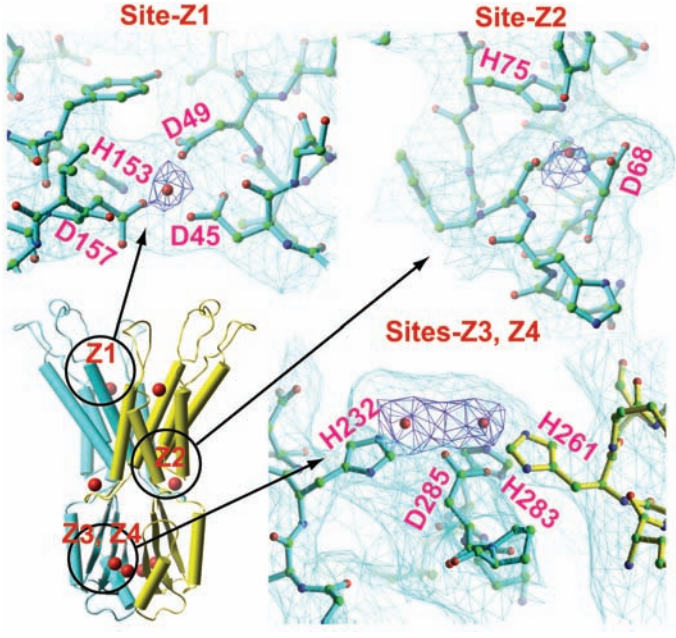

Fig. 4. Zn^{2+} binding sites. Zn^{2+} ions are represented by red spheres. The overall locations of sites Z1 to Z4 in the Yiip dimer are circled. Protein residues (cyan and yellow) and their experimental electron densities (light cyan) at 1.2 σ contour levels overlay zinc difference anomalous Fourier maps (blue) contoured at 3.5 σ, 4.0 σ, and 6.0 σ for sites Z1, Z2, and Z3-Z4, respectively.

References and Notes

1. B. L. Vallee, K. H. Falchuk, *Physiol. Rev.* **73**, 79 (1993).
2. J. M. Berg, Y. Shi, *Science* **271**, 1081 (1996).
3. K. Hirzel *et al.*, *Neuron* **52**, 679 (2006).
4. C. J. Frederickson, A. Bush, *Biometals* **14**, 353 (2001).
5. G. Dodson, D. Steiner, *Curr. Opin. Struct. Biol.* **8**, 189 (1998).
6. J. Y. Koh *et al.*, *Science* **272**, 1013 (1996).
7. A. I. Bush *et al.*, *Science* **265**, 1464 (1994).
8. J. Y. Lee *et al.*, *Proc. Natl. Acad. Sci. U.S.A.* **99**, 7705 (2002).
9. C. E. Outten, T. O'Halloran, *Science* **292**, 2488 (2001).
10. R. D. Palmiter, S. Findley, *EMBO J.* **14**, 639 (1995).
11. D. H. Nies, S. Silver, *J. Ind. Microbiol.* **14**, 186 (1995).
12. T. B. Cole *et al.*, *Proc. Natl. Acad. Sci. U.S.A.* **96**, 1716 (1999).
13. F. Chimienti *et al.*, *J. Cell Sci.* **119**, 4199 (2006).
14. R. Sladek *et al.*, *Nature* **445**, 881 (2007).
15. Y. Wei, H. Li, D. Fu, *J. Biol. Chem.* **279**, 39251 (2004).
16. Y. Wei, D. Fu, *J. Biol. Chem.* **280**, 33716 (2005).
17. Y. Wei, D. Fu, *J. Biol. Chem.* **281**, 23492 (2006).
18. G. Grass *et al.*, *J. Bacteriol.* **183**, 4664 (2001).
19. G. Grass *et al.*, *Arch. Microbiol.* **183**, 9 (2005).
20. Materials, methods, and structure statistics are available as supporting material on *Science* Online.
21. A. K. Wernimont *et al.*, *Nat. Struct. Biol.* **7**, 766 (2000).
22. A. C. Rosenzweig, T. V. O'Halloran, *Curr. Opin. Chem. Biol.* **4**, 140 (2000).
23. L. A. Finney, T. V. O'Halloran, *Science* **300**, 931 (2003).
24. T. E. Furia, *Handbook of Food Additives* (CRC Press, Cleveland, ed. 2, 1980).
25. Y. Chao, D. Fu, *J. Biol. Chem.* **279**, 17173 (2004).
26. A. Anton *et al.*, *J. Bacteriol.* **186**, 7499 (2004).
27. I. T. Paulsen, M. J. Saier, *J. Membr. Biol.* **156**, 99 (1997).

28. We thank A. Heroux, A. Soares, and A. Saxena for assistance in data collection and J. Shanklin, P. Freimuth, P. Maloney, and C. Anderson for comments. This work was supported by the National Institutes of Health (D.F.) and the Biology Department of Brookhaven National Laboratory, U.S. Department of Energy. The coordinates for the structure have been deposited in the Protein Data Bank under the accession code 2QFI.

Supporting Online Material

www.sciencemag.org/cgi/content/full/1143748/DC1
Materials and Methods
Figs. S1 to S3
Tables S1 and S2
References

12 April 2007; accepted 7 August 2007
Published online 23 August 2007;
10.1126/science.1143748
Include this information when citing this paper.